Am J Physiol Cell Physiol 286: C1434–C1442, 2004.
First published February 11, 2004; 10.1152/ajpcell.00539.2003.

Immunocytochemical localization of Na^+-HCO_3^- cotransporters and carbonic anhydrase dependence of fluid transport in corneal endothelial cells

Friedrich P. J. Diecke,[1] Quan Wen,[2] Jose M. Sanchez,[2] Kunyan Kuang,[2] and Jorge Fischbarg[2,3]

[2]Ophthalmology and [3]Physiology and Cellular Biophysics, Columbia University, New York, New York 10032; and [1]Department of Pharmacology and Physiology, University of Medicine and Dentistry of New Jersey-New Jersey Medical School, Newark, New Jersey 07103

Submitted 2 December 2003; accepted in final form 6 February 2004

Diecke, Friedrich P. J., Quan Wen, Jose M. Sanchez, Kunyan Kuang, and Jorge Fischbarg. Immunocytochemical localization of Na^+-HCO_3^- cotransporters and carbonic anhydrase dependence of fluid transport in corneal endothelial cells. *Am J Physiol Cell Physiol* 286: C1434–C1442, 2004. First published February 11, 2004; 10.1152/ajpcell.00539.2003.—In corneal endothelium, there is evidence for basolateral entry of HCO_3^- into corneal endothelial cells via Na^+-HCO_3^- cotransporter (NBC) proteins and for net HCO_3^- flux from the basolateral to the apical side. However, how HCO_3^- exits the cells through the apical membrane is unclear. We determined that cultured corneal endothelial cells transport HCO_3^- similarly to fresh tissue. In addition, Cl^- channel inhibitors decreased fluid transport by at most 16%, and inhibition of membrane-bound carbonic anhydrase IV by benzolamide or dextran-bound sulfonamide decreased fluid transport by at most 29%. Therefore, more than half of the fluid transport cannot be accounted for by anion transport through apical Cl^- channels, CO_2 diffusion across the apical membrane, or a combination of these two mechanisms. However, immunocytochemistry using optical sectioning by confocal microscopy and cryosections revealed the presence of NBC transporters in both the basolateral and apical cell membranes of cultured bovine corneal endothelial cells and freshly isolated rabbit endothelia. This newly detected presence of an apical NBC transporter is consistent with its being the missing mechanism sought. We discuss discrepancies with other reports and provide a model that accounts for the experimental observations by assuming different stoichiometries of the NBC transport proteins at the basolateral and apical sides of the cells. Such functional differences might arise either from the expression of different isoforms or from regulatory factors affecting the stoichiometry of a single isoform.

confocal microscopy; cryosections; stoichiometry; pH titration; chloride channels

THE BICARBONATE ION (HCO_3^-) appears to be central to fluid transport across corneal endothelium; the fact that its presence in the medium is required has been well documented (12, 18, 22). Net HCO_3^- flux from the stromal to the aqueous side across rabbit corneal endothelium has been reported (18, 19). In addition, that flux is in all likelihood transcellular, given that it takes place against a small but significant voltage gradient across the endothelium (~500 μV, aqueous negative; Refs. 4, 11, 12, 17). For transcellular flux, HCO_3^- would have to enter the cell via the basolateral membrane against a voltage gradient (intracellular potential −45 mV; Ref. 24) and exit via the apical membrane. There is evidence that the entry step involves secondary active transport across a Na^+-HCO_3^- cotransporter (NBC) in that removal of external Na^+ led to acidification (7, 37) and a NBC has been located by immunocytochemistry in the basolateral membrane (but not in the apical membrane) by Sun et al. (37) and Bok et al. (5). On the other hand, the mechanism by which HCO_3^- exits the cell is less clear. Jentsch and colleagues (20) proposed a Na^+-HCO_3^--coupled exit. Bonanno and Giasson (7) gave arguments for an alternative mechanism based on a role of an apical Cl^-/HCO_3^- exchanger. Recently, however, the same laboratory (6) demonstrated that the anion exchanger is actually located in the lateral membrane and thus cannot mediate HCO_3^- exit through the apical membrane. These authors propose currently that HCO_3^- exits the cell via the cystic fibrosis transmembrane conductance regulator (CFTR) (36) and calcium-activated chloride channels (CaCC) (43). In addition, they postulate that CO_2 diffuses across the apical membrane, because of a CO_2 gradient established by the combined action of a cytoplasmic carbonic anhydrase (CA) II catalyzing dehydration of HCO_3^- and an extracellular membrane-bound CA IV (31) catalyzing hydration of CO_2 into HCO_3^- (6, 8).

We recently reexamined the question of apical exit of HCO_3^- and, from theoretical considerations (unpublished observations), determined that for proper balance of electrical and chemical fluxes across these cells, coupled Na^+-HCO_3^- apical exit [as postulated by Jentsch et al. (20)] could not be discarded. Moreover, we report here that inhibition of Cl^- channels as well as selective inhibition of the membrane-bound CA IV with impermeant CA inhibitors result in only small changes in corneal endothelial fluid transport and thus do not appear to be the major driving forces for it. In the search for other mechanisms for fluid transport, we therefore set out to examine the distribution of NBC proteins in cultured and fresh corneal endothelial cells. Here we present evidence that both basolateral and apical membranes express an NBC protein, and we discuss how different stoichiometries (2:1 entry, 3:1 exit) might underlie transcellular HCO_3^- flux.

MATERIALS AND METHODS

Cell culture. Corneal endothelial cells were cultured and subcultured as described previously (9). Cells reached confluence in 5–7 days, after which they were subcultured. For immunocytochemistry experiments cells were subcultured into two-well chamber slide systems (Nunc, Naperville, IL), and for the HCO_3^- flux measurements cells were subcultured on 25-mm Costar permeable inserts until 2–3 days after confluence. Confluence was checked visually under a phase-contrast inverted microscope (Nikon TMS, ×200) and by measuring the transendothelial resistance with an Endohm-24 tissue

Address for reprint requests and other correspondence: J. Fischbarg, Dept. of Physiology and Cellular Biophysics, Coll. of P & S, Columbia Univ., 630 West 168th St., New York, NY 10032 (E-mail: jf20@columbia.edu).

The costs of publication of this article were defrayed in part by the payment of page charges. The article must therefore be hereby marked "*advertisement*" in accordance with 18 U.S.C. Section 1734 solely to indicate this fact.

resistance measurement chamber (WPI, Sarasota, FL) in conjunction with an EVOM epithelial voltohmeter (WPI).

Corneal tissue preparation. Bovine eyes were obtained from an abattoir as previously described (9). Before dissection, the ocular globes were washed with PBS. The globes were placed in a petri dish, and the corneas were dissected off. Corneas were then washed twice with a HEPES-buffered Hanks' balanced salt solution (medium 199; catalog no. 12350, GIBCO-BRL) and were cut in rectangular pieces of ~1 × 0.5 cm. These pieces were then washed three times with medium 199 at 37°C and fixed as described in *Immunocytochemistry*.

Immunocytochemistry. Cultured bovine corneal endothelial cells (CBCEC) subcultured as described in *Cell culture* were washed twice with medium 199 at 37°C, fixed for 30 min in PLP fixative (2% formaldehyde, 75 mM lysine, 10 mM sodium periodate, 45 mM sodium phosphate, pH 7.4; Ref. 28), washed in Dulbecco's PBS (GIBCO-BRL) three times, permeabilized with 0.075% saponin in PBS for 20 min, and washed again in PBS three times. The cells were then incubated for 1 min in a 1% solution of sodium dodecyl sulfate (SDS) in PBS. The cell monolayers were then incubated in blocking solution (15% goat serum, 0.3% Triton X-100, 20 mM sodium phosphate, 0.9 mM sodium chloride; Ref. 25) for 30 min. After the blocking solution was removed by aspiration, the monolayers were exposed to a rabbit anti-NBC polyclonal antibody (catalog no. AB3204, Chemicon International, Temecula, CA), which recognizes the rat kidney NBC-1 COOH terminus amino acids 990–1035 segment, or to another rabbit anti-NBC polyclonal antibody (also from Chemicon, catalog no. AB3212), which recognizes the rat kidney NBC-1 NH_2 terminus amino acids 338–391 segment. The antibodies were diluted in PBS plus 15% goat serum and 0.2% bovine serum albumin (Sigma, St. Louis, MO) in PBS. After trying a range of concentrations, we settled on a dilution of 1:500 for the primary antibody (final concentration 2 μg/ml). As a control, in given experiments, we preabsorbed with the immunogenic NBC COOH-terminal peptide (amino acids 990–1035; synthesized for us by Alpha Diagnostics International, San Antonio, TX). The final concentration of the peptide was 2 μg/ml (in PBS). The incubations were done for 60 min in a humid chamber at room temperature. Subsequently, the cell layers were washed three times in PBS and twice in PBS plus 5% goat serum (5–10 min each time). The cell layers were then incubated in rhodamine red-X-conjugated goat anti-rabbit IgG (Jackson ImmunoResearch Laboratories, West Grove, PA) at a dilution of 1:200 (in PBS) for 90 min in the same humid chamber at room temperature. Samples were prepared and kept in the dark to prevent light-induced damage to rhodamine red-X.

Tissue preparation. Corneal tissue samples were fixed in PLP medium for 1 h and were washed in PBS three times. They were then immersed in 30% sucrose and kept overnight at 4°C. Subsequently the excess solution was absorbed away, and the pieces were embedded in optimal cutting temperature (OCT) compound (Tissue-Tek; Sakura Finetek, Torrance, CA). The pieces were kept in a freezer at −20°C and were subsequently sectioned in a cryostat (CM 1850, Leica Microsystems, Bannockburn, IL; 4-μm-thick specimens). Specimens were collected on Silane-Prep slides (Sigma). The rest of the procedure was the same as described for the cultured cells, including permeabilization, denaturation, and blocking. For control experiments once more we used the antigen peptide.

Nuclear counterstaining and mounting. Samples were equilibrated briefly in 2× SSC solution (300 mM sodium chloride, 30 mM sodium citrate, pH 7.0 titrated with HCl) and then incubated for 20 min in 2× SSC solution containing 5 μg/ml DNase-free RNase (Boehringer Mannheim, Indianapolis, IN). Incubation was terminated with three washes in 2× SSC solution (1 min each), after which samples were incubated for 5 min in Sytox green (Molecular Probes, Eugene, OR) diluted 1:300 (vol/vol) in 2× SSC solution and then rinsed five times (1 min each) in 2× SSC solution. The upper part of the chamber slide system was then quickly removed, leaving only the cells on the slides. Finally, coverslips were applied to the samples with 1 drop per well of H-1000 Vectashield Mounting Medium (Vector Laboratories, Burlingame, CA). The excess mounting medium was aspirated, and the coverslips were secured with clear nail polish.

The preparations were screened for fluorescence with an Axiovert S100 microscope (Carl Zeiss, Thornwood, NY) using excitation wavelengths of 480 and 545 nm to detect emission by nuclear staining (Sytox green) or antibody staining (rhodamine red-X), respectively. Preparations showing staining were then examined with a scanning confocal microscope (LSM 410, Carl Zeiss). Excitation came from its argon-krypton laser, producing lines at 488 or 568 nm. Fluorescence in the *x-y* plane was recorded at different depths, and fluorescence in the *x-z* and *y-z* planes was obtained from the combined *x-y* images with Zeiss LSM-PC software. The images were enhanced with Adobe Photoshop software (San Jose, CA).

Transendothelial HCO_3^- flux measurements. The HCO_3^- flux across cultured bovine endothelial cell monolayers was measured with a pH-stat method adapted and modified from van Adelsberg et al. (42). Permeable tissue culture inserts with confluent monolayers were mounted in a modified Ussing chamber (Fig. 1) consisting of two compartments separated by the insert membrane and the cell monolayer. Each compartment was connected to a reservoir, and solutions from the reservoirs circulated continuously through the compartments with the aid of an airlift system so that the chamber volume was exchanged once every 15 s. One compartment of the Ussing chamber was perfused with a HCO_3^--CO_2-buffered solution aerated with a mixture of 5% CO_2 and 95% air, whereas the other compartment was perfused with a solution nominally free of HCO_3^- and CO_2, which was vigorously bubbled with CO_2-free air and buffered with a low-concentration (0.1 mM) phosphate buffer. Except where noted, the detailed composition of the HCO_3^--CO_2-buffered solution (*solution II*) was (in mM) 126.5 NaCl, 4.8 KCl, 1.7 $CaCl_2$, 1.0 $MgSO_4$, 1.0 NaH_2PO_4, 26.2 $NaHCO_3$, and 5.5 glucose; pH was 7.4. The HCO_3^--CO_2-free solution (*solution I*) contained (in mM) 154 NaCl, 4.8 KCl, 1.7 $CaCl_2$, 1.0 $MgSO_4$, 0.066 Na_2HPO_4, 0.033 NaH_2PO_4, and 5.5 glucose (pH 7.4). With this arrangement, CO_2 and HCO_3^- diffused from *solution II* to *solution I* in parallel with any active transendothelial transport. In the phosphate-buffered compartment (*solution I*), the CO_2 was driven off by the CO_2-free air and the pH change resulting from the accumulating HCO_3^- was detected by a pH electrode and a pH meter. Because the pH of the compartment became more alkaline than the control pH (7.4, unless specified), the voltage

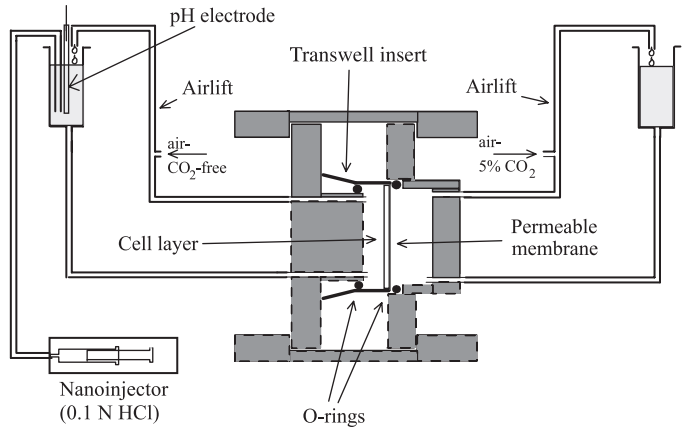

Fig. 1. pH-stat type setup to determine HCO_3^- fluxes. The cultured cells are grown on the permeable insert shown clamped in a Lucite chamber (cross section of the chamber is shown in gray). Each half of the chamber is superfused separately by way of the Ussing-type airlifts depicted. The pH electrode is connected to a high-impedance voltmeter (not shown); the output of the voltmeter goes to a comparator (not shown). As HCO_3^- flows into the target chamber, pH rises; the resulting voltage change triggers the comparator-injector on and off so as to keep pH between 7.4 and 7.48.

output from the pH meter differed from a set level, triggering a stepping motor that in turn drove a microsyringe injecting 1 M HCl into the *solution I* compartment until its pH returned to the control value. Each step of the motor injected 1 nmol of HCl into *solution I*; the amount of steps accumulated was displayed on a LED display reset every 30 min. This automatic titration system maintained the pH of *solution I* constant within 0.08 pH units.

The HCO_3^- unidirectional fluxes were calculated as

$$HCO_3^- \text{ flux} = \frac{n \text{ (injection steps)} \times 1 \frac{\text{nmol}}{\text{step}} \times 60 \frac{\text{min}}{\text{h}}}{\text{area of monolayer} \times 30 \text{ min}} \quad (1)$$

The HCO_3^- flux was measured in the basolateral-to-apical and apical-to-basolateral directions alternatively during a same experiment, by placing *solution I* in the target compartment and *solution II* in the contralateral compartment. The difference of fluxes in these two directions was assumed to be the transendothelial HCO_3^- flux resulting from membrane transport mechanisms.

A possible error of this method is due to the reversible reaction of CO_2 diffusing from *solution II* to *solution I* to yield carbonic acid followed by subsequent dissociation of carbonic acid to H^+ and HCO_3^-. This error was kept low by bubbling the *solution I* vigorously with CO_2-free air so as to maintain P_{CO_2} as close to zero as possible. Moreover, because the hydration reaction is much slower than the dehydration reaction, the probability that some HCO_3^- is converted to CO_2 and removed in the CO_2-free atmosphere is higher than for the reverse reaction. This would then lead to an underestimate of the unidirectional HCO_3^- fluxes. However, because the transendothelial HCO_3^- transport is calculated as the difference of the unidirectional fluxes in the basolateral-to-apical and apical-to-basolateral directions, the errors would tend to cancel out.

Transendothelial fluid transport measurements. The putative role of the Cl^- channels and CO_2 diffusion in the generation of fluid transport was investigated by the Maurice-Dikstein method (10), a method that determines fluid transport by monitoring corneal thickness. Corneal thickness is a function of the imbibition pressure generated by the stromal glycosaminoglycans, which drives fluid into the stroma, and by the fluid secretion mechanism of the corneal endothelium. In the physiologically stable cornea, these two mechanisms are equal so that there is no net fluid transport and no change in corneal thickness. However, any change in endothelial ion and fluid transport will be reflected in a change of corneal thickness.

Rabbit corneas were obtained from New Zealand albino rabbits (~2 kg). Animal procedures were in accordance with the *Guide for the Care and Use of Laboratory Animals* (NIH Pub. No. 85-23, revised 1985). Rabbits were euthanized with an overdose of pentobarbital sodium solution (Butler, Columbus, OH) injected into the marginal ear vein. The eyes were enucleated immediately by the technique of Dikstein and Maurice (10). The deepithelialized cornea was mounted in a Dikstein-Maurice chamber held in a thermal jacket kept at 36.5°C and viewed with a specular reflection microscope (10). The endothelial side of the cornea was superfused with solutions at a rate of 1.4 ml/h by a syringe pump (Razel Scientific Instruments, Stamford, CT), whereas the stromal surface was covered with silicone oil. Stromal thickness was measured in the conventional fashion (2) by focusing in sequence on the stroma-oil and endothelium-fluid interfaces and using the microscope micrometer to gauge their separation. Readings were taken every 15 min for 4 h.

For endothelial superfusion, the medium used was a HEPES-HCO_3^- Ringer solution containing (in mM) 104.4 NaCl, 26.2 $NaHCO_3$, 3.8 KCl, 1 KH_2PO_4, 0.8 $MgSO_4$, 1.7 $CaCl_2$, 6.9 glucose, and 20 HEPES. The pH was 7.4, and the osmolality was 290 mosmol/kgH_2O. Ouabain, 5-nitro-2-(3-phenylpropylamino)benzoic acid (NPPB), and parabromophenacyl bromide (pBPB) were from Sigma. The specific CFTR inhibitor (26) was a gift of Dr. Alan Verkman (University of California, San Francisco, CA). Benzolamide was kindly supplied by Dr. Eric Swenson (University of Washington, Seattle, WA); we also used dextran-bound acetazolamide (Synthelec, Lund, Sweden). CA was from bovine erythrocytes (catalog no. 215755, Calbiochem, La Jolla, CA). Stock solutions of the reagents were obtained by dissolving them in dimethyl sulfoxide (DMSO) (except for ouabain, which was dissolved in Ringer solution). The final concentration of DMSO in the superfusion medium was kept at ≤0.1%.

RESULTS

HCO_3^- fluxes. Rabbit corneal endothelial preparations exhibit net translayer transport of HCO_3^- (18, 19). As for the cultured endothelial cells used extensively by other laboratories and ourselves, because there is evidence that they transport fluid [bovine (29), human (1)], they would also be expected to transport HCO_3^-. However, because this has not been documented, we set out to determine it. The pH-stat method we chose appears convenient in that it does not require isotopes or a closed system.

In a typical experiment, HCO_3^- flux from the apical to the basolateral side (presumed direction of the leak) was measured for a period of 30 min. The solutions were then replaced on both sides of the preparation so as to determine HCO_3^- flux in the opposite direction (from basolateral to apical, with the expectation of determining active transport plus leak) again for 30 min. This was then followed by yet another solution exchange and a determination of apical-to-basolateral flux for 30 min. Thus there were two measurements of the presumed leak bracketing the measurement of active transport plus leak. We took the average of the two leak measurements and subtracted it from the basolateral-to-apical flux, which gave us the putative transcellular net HCO_3^- flux for that experiment. Figure 2 shows the values for the unidirectional fluxes (basolateral to apical and apical to basolateral) and the net fluxes. The HCO_3^- flux from the basolateral to the apical side was consistently greater than the reverse flux, resulting in a statistically significant net flux of 0.53 ± 0.07 $\mu eq \cdot h^{-1} \cdot cm^{-2}$ (Fig. 2). In addition, from the passive unidirectional flux values for the cell monolayer on its insert and the insert alone and the HCO_3^- concentration ($[HCO_3^-]$) gradient, we calculated the permeability of the cell monolayer to HCO_3^- to be 4.8 (±0.2) × 10^{-5} cm/s.

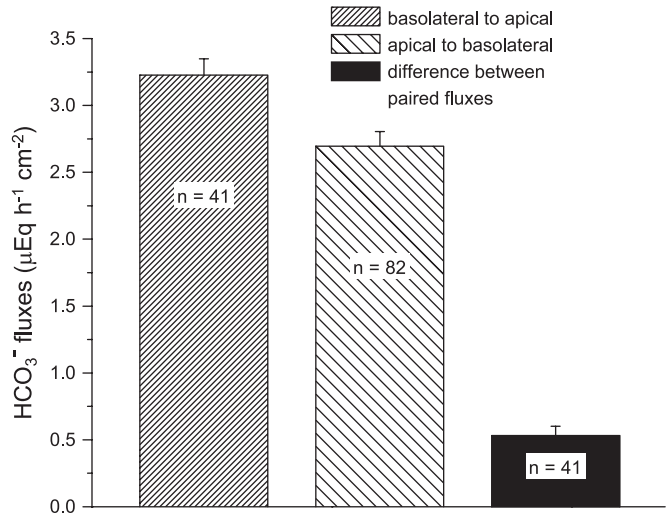

Fig. 2. Summary of measurements of unidirectional and net HCO_3^- fluxes (averages ± SE). Nos. of measurements are given inside bars.

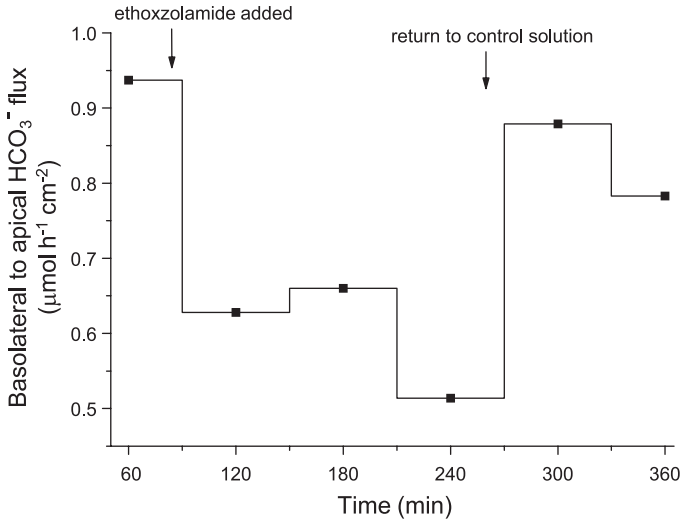

Fig. 3. Effect of the addition of 0.1 mM ethoxyzolamide to both sides of the chamber in an experiment (typical of 4) in which the unidirectional flux indicated was determined. Points denote the centers of the 30-min time intervals during which fluxes were determined.

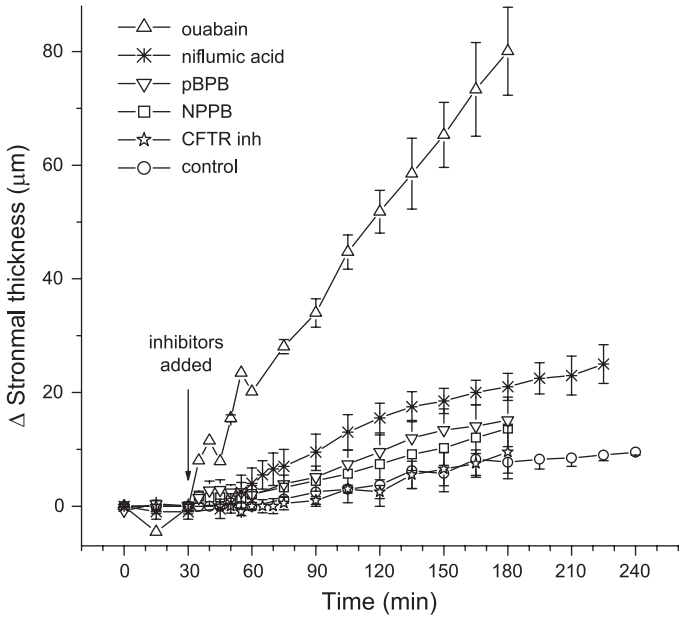

Fig. 4. Net fluid movements across corneal endothelium as determined by changes (Δ) in stromal thickness (Dikstein-Maurice technique): comparison of the effects of ouabain (maximal inhibition of fluid transport) with those of Cl^- channel inhibitors. Each curve presents average ± SE values for 4 experiments. pBPB, parabromophenacyl bromide; NPPB, 5-nitro-2-(3-phenylpropylamino)benzoic acid; CFTR inh, cystic fibrosis transmembrane conductance regulator inhibitor.

To further characterize these fluxes, we investigated the effect of the CA inhibitor ethoxyzolamide on them. For this purpose, with conditions similar to those described above, it was not possible to detect a statistically significant inhibition because of the variability of the two large unidirectional fluxes (cf. Fig. 2). To obviate this, we sought to reduce the unidirectional fluxes by decreasing the [HCO_3^-] to 9.2 mM in *solution II* while keeping the P_{CO_2} constant in that solution by bubbling with 5% CO_2. As a result, the pH of *solution II* became 7.0, and this meant that the phosphate buffer in *solution I* had to be adjusted to 7.0, which was the set point pH for this series. A representative experiment is shown in Fig. 3; as can be seen in that figure, the inhibitor at a high concentration (0.1 mM) results in a large but reversible inhibition of the unidirectional flux. These experiments suggest that cellular CA is capable of contributing to HCO_3^- flux under those particular conditions, namely, low ambient [HCO_3^-] and normal P_{CO_2}. Because $CO_2 + OH^- \leftrightarrow HCO_3^-$, the intracellular CA II-driven reaction from left to right would gain importance at lower [HCO_3^-], in agreement with our observation. This issue may be further illuminated by our consideration of the roles of the intracellular and extracellular CAs as described for the alternate model for the anion pathway in DISCUSSION.

Cl^- channel inhibition. It has been postulated that one of the two pathways for the passage of HCO_3^- across the apical membrane of corneal endothelial cells is via Cl^- channels. Two types of these channels have been identified in corneal endothelial cells, calcium-activated Cl^- channels (CaCC; Ref. 43), and CFTRs (36). We have examined the role of Cl^- channels in fluid transport by using a number of Cl^- channel inhibitors and the Dikstein-Maurice technique. Figure 4 compares the effects of several of these inhibitors on corneal thickness, NPPB, pBPB, a specific CFTR inhibitor, and niflumic acid, with the rates of swelling obtained in ouabain (1 mM) and the spontaneous swelling in control solution. Ouabain affected a rapid equilibration of all intracellular electrolyte concentrations, abolished the membrane and transendothelial potential differences, and thus inhibited the transendothelial fluid transport completely. The rate of swelling (32.3 μm/h) observed in ouabain solutions reflects a fluid leak of 3.23 μl/h from the aqueous side to the stromal side due to the imbibition pressure of the stroma. This fluid leak was not completely compensated in control solution, and there remained a spontaneous rate of swelling of 3.2 μm/h. The transendothelial fluid transport under in vitro conditions was therefore 2.91 μl/h. In solutions containing the Cl^- channel inhibitors NPPB or pBPB (Fig. 5) at maximally effective concentrations (100 μM), the

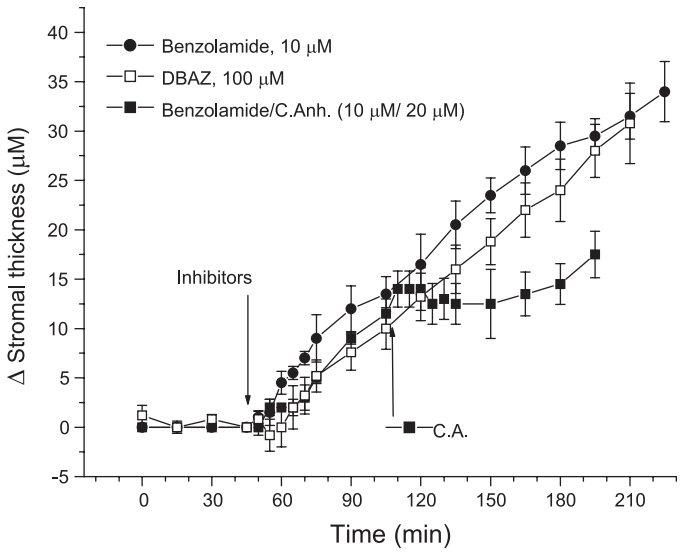

Fig. 5. Effects of inhibitors of extracellular membrane-bound carbonic anhydrase (CA) IV on fluid transport. In one of the series of experiments, after benzolamide inhibition, CA was added to the superfusion medium. Technique and nos. of experiments are as in Fig. 4. DBAZ, dextran-bound acetazolamide.

rate of swelling increased at an average of 6.2 μm/h, corresponding to a reduction of transendothelial fluid transport to 2.61 μl/h, a 10.3% decrease from control. The CFTR inhibitor had no significant effect compared with spontaneous swelling, whereas niflumic acid, a compound used to inhibit the CaCC (43), reduced the transendothelial fluid transport by ~16%.

Inhibition of apical extracellular CA IV. The apical membrane of corneal endothelial cells possesses a membrane-bound extracellular CA IV (31). It has been proposed that this CA establishes a transcellular CO_2 gradient by catalyzing the conversion of CO_2 to HCO_3^- and thus effectively generating a HCO_3^- flux across the endothelial cells. We have examined the possible role of CA IV in transendothelial fluid transport by inhibiting the enzyme with the relatively impermeant CA inhibitor benzolamide and an impermeant dextran-bound sulfonamide. The results are summarized in Fig. 5. Benzolamide, at the supramaximal concentration of 10 μM, produced a rate of swelling of 11.3 μm/h. This corresponds to a reduction of transendothelial fluid transport by 0.81 μl/h, or 27.8%. Increasing the benzolamide concentration to 30 μM reduced fluid transport by the same amount. When the swelling initiated by benzolamide was interrupted by switching to a solution containing CA, to absorb any residual inhibitor and restore CA activity, the swelling stopped immediately. This indicates that benzolamide indeed inhibits an extracellular CA. The results obtained with benzolamide were confirmed with an impermeant dextran-bound CA inhibitor of mol wt 7,000, which at the concentrations of 0.1 and 1 mM produced a rate of swelling corresponding to a reduction of fluid transport by 0.67 μl/h, or 22.8%.

Localization of NBC: cultured cells. We investigated the localization of NBC both in cultured cells and in fresh corneal tissue slices. Figure 6 depicts selected images of a gallery of optical sections of CBCEC obtained by confocal microscopy. Evidence for the presence of NBC is seen at the level of the apical membrane (Fig. 6, *a* and *b*), lateral membrane (Fig. 6*c*), and lateral and basal membrane (Fig. 6*d*). The three-dimensional reconstruction shown in Fig. 7 reinforces this view. Figure 7*b*, the *x–z* reconstruction, is especially noteworthy in that the stained membrane envelope all around a cell is clearly noticeable. There is also some diffuse staining of the cytoplasm. This gallery is representative of 11 galleries obtained in cells from two different batches of bovine eyeballs.

Localization of NBC: tissue slices. Because it is conceivable that expression of given proteins and/or their isoforms could be different in proliferating cultured cells from that in fresh tissue cells, we investigated the localization of NBC in bovine corneal cryosections. The results in Fig. 8 once more show evidence for the localization of NBC in both apical and basolateral endothelial cell membranes. The staining in the apical membrane region is significantly less than that in the basolateral membrane, indicating a lower density of transport proteins. These data are representative of 23 cryosections obtained from 10 corneas.

Finally, for control purposes, we preabsorbed the antigenic peptide and subjected sections to the same procedures as above

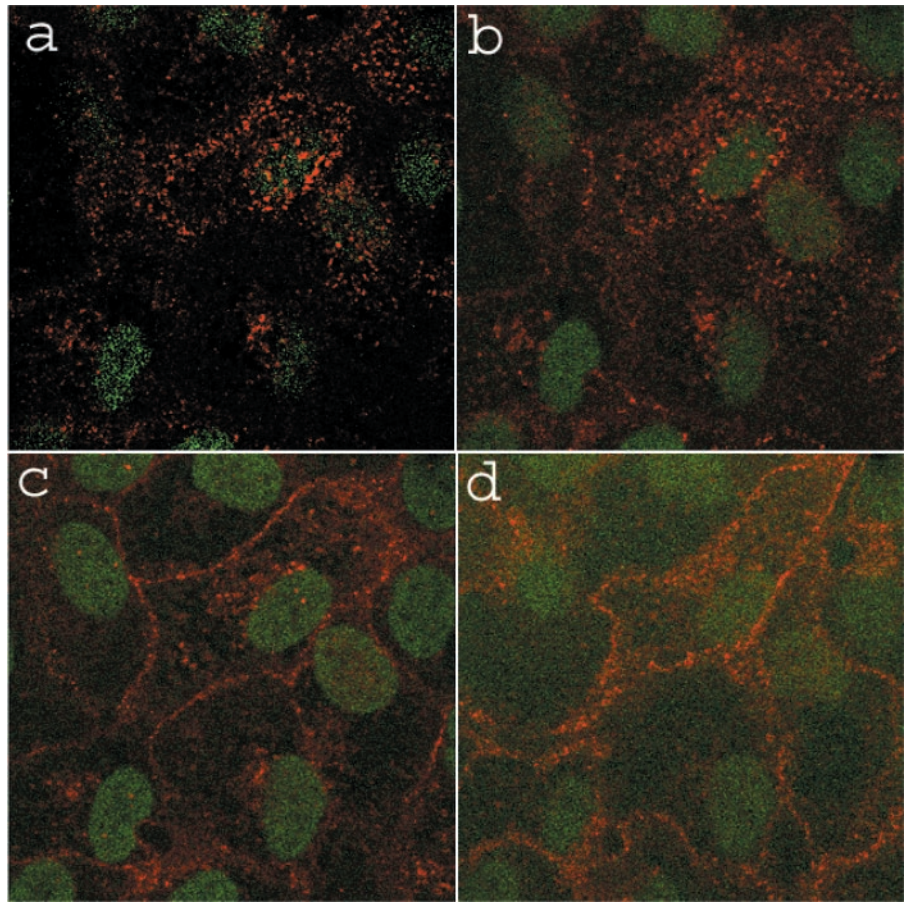

Fig. 6. Immunofluorescence localization of Na^+-HCO_3^- cotransporter (NBC) in cultured bovine corneal endothelial cells (CBCEC). Serial confocal optical sections (45.1-μm squares) from a plane just at the apical membrane to the basal membrane (*left* to *right*, *top* to *bottom*). Red, labeling with NBC antibody and rhodamine-conjugated secondary antibody; green, Sytox green-stained nuclei. From images at 12 levels, 4 are shown. *a*: At the level of the apical membrane above the nucleus. *b*: Through the top of the nucleus, showing the apical membrane sloping down. *c*: Through the lateral membrane. *d*: Near the basal membrane. NBC is in both the apical membranes (*a*, *b*) as well as in the lateral (*c*, *d*) and basal (*d*) membranes.

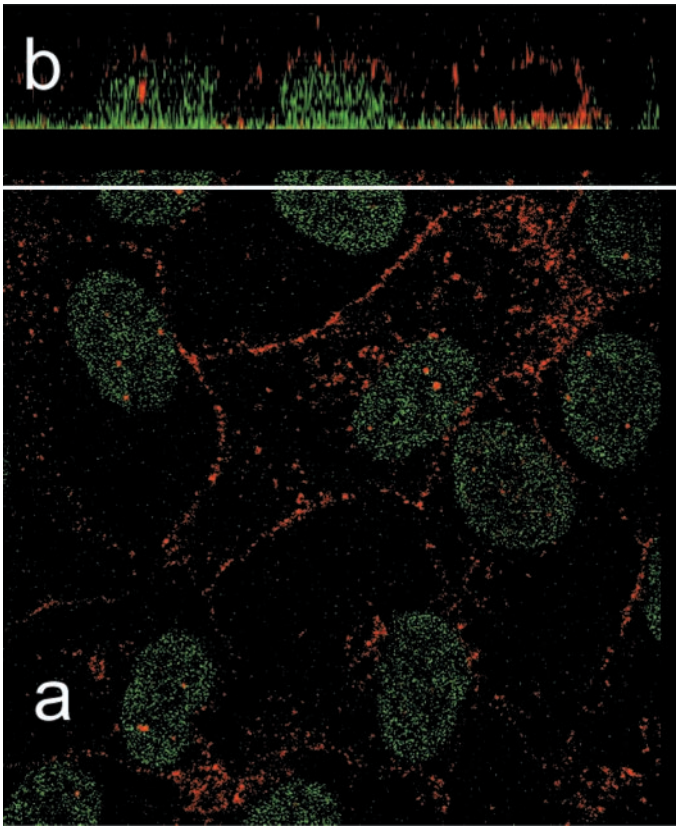

Fig. 7. Three-dimensional reconstruction of CBCEC. *a*: Cross section of the cell layer that corresponds to *frame c* of the gallery in Fig. 6 (side length 45.1 μm). *b*: *x*–*z* section for the plane marked with the white line, obtained with Zeiss LSM-PC software from the gallery of images summarized in Fig. 6.

(not shown). No staining for NBC was evident, whereas all other corneal structures were clearly visible (3 sections in a cornea that evidenced clear NBC staining without preabsorption).

DISCUSSION

HCO_3^- fluxes. As mentioned above, the net HCO_3^- flux we determined was 0.53 ± 0.07 $\mu eq \cdot h^{-1} \cdot cm^{-2}$. This value is comparable to that (0.67 ± 0.11 $\mu eq \cdot h^{-1} \cdot cm^{-2}$) reported by Hodson and Miller (18). It should be noted that they used rabbit corneal endothelial preparations and we used cultured bovine cells. In addition, their ambient [HCO_3^-] of 37 mM was higher than the 26 mM we used for these experiments. The value for net HCO_3^- flux found by Green and colleagues (19) was much larger (2.5 ± 0.2 $\mu eq \cdot h^{-1} \cdot cm^{-2}$). Assuming tight isotonic coupling between electrolyte net fluxes and water flows, fluxes of the order of 0.53–0.67 $\mu eq \cdot h^{-1} \cdot cm^{-2}$ would correspond to flows of ~3.5–4.5 $\mu l \cdot h^{-1} \cdot cm^{-2}$. These values agree with the order of the values experimentally determined for isolated rabbit corneal preparations in Ussing chambers modified for flow measurements [in $\mu l \cdot h^{-1} \cdot cm^{-2}$: ~6.0 (27) and 4.5 (13)]. Larger HCO_3^- flux values (19) would entail either looser coupling or much larger fluid flows than those determined so far. The value of the permeability of the cell monolayer to HCO_3^- was 4.8 ± 0.2 × 10^{-5} cm/s. This is of the same order of magnitude as a value of 2.1 ± 0.2 × 10^{-5} cm/s reported by Hodson and Miller (18) for the deepithelialized rabbit cornea.

These observations justify the conclusion that the cultured cells are polarized and exhibit net HCO_3^- transport that would correspond to a distribution and a density of expression of HCO_3^- transporters similar or identical to those of fresh tissue. This net HCO_3^- transport would then form part of the fluid transport machinery in this layer; a recent model (33) includes a role for electrogenic transcellular HCO_3^- transport in electroosmosis-driven transendothelial fluid transport.

Inhibition of Cl^- channels. Several types of anion channels have been described for corneal endothelial cells. These channels include a large-conductance nonspecific anion channel identified by patch-clamp studies (30), which is inoperative at resting membrane potential. In addition, RT-PCR screening has revealed the presence and activation of CFTR (38) and CaCC (43) channels in the bovine corneal endothelium.

Inhibition of Cl^- channels with a range of different Cl^- channel inhibitors (Fig. 4) consistently showed only relatively small effects on transendothelial fluid transport, ranging from insignificant to a maximum of 16%. The contribution of apical Cl^- channels to transendothelial fluid transport is of the same order of magnitude as that of the basolateral Na^+-K^+-$2Cl^-$ cotransporter (NKCC) (21), suggesting the existence of a small vectorial Cl^- transport from the basolateral to the apical side.

Inhibition of CA IV. The corneal endothelium possesses a membrane-bound extracellular CA IV (31), which is confined to the apical membrane (6). It has been hypothesized that this

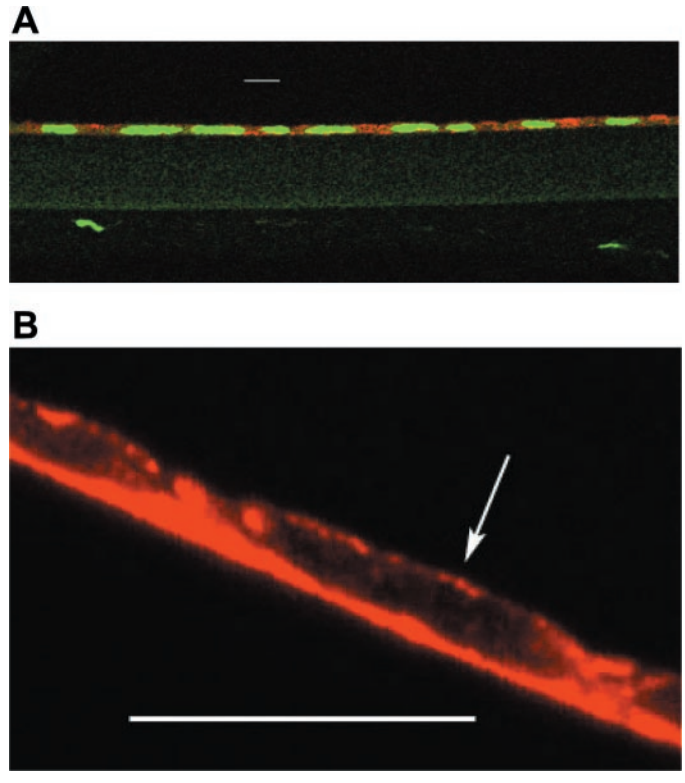

Fig. 8. Two cryosections across fresh bovine cornea. Colors and stains are as in Figs. 6 and 7. Bars represent 10 μm. *A*: the corneal endothelium plus a segment of the underlying Descemet membrane and stroma. Note that keratocyte nuclei are visible; rhodamine fluorescence is detected only in endothelial cells. *B*: the preparation was illuminated with the 568-nm wavelength. Staining is seen in both apical (arrow) and basolateral membranes.

CA IV catalyzes the hydration of CO_2 to HCO_3^- in the unstirred layer adjacent to the apical membrane and thus creates a stromal-to-aqueous CO_2 gradient; it has been postulated that this is one of the pathways that contribute to transcellular HCO_3^- flux and fluid transport (8). We have examined this hypothesis by determining the effect of selective inhibition of the extracellular CA IV, and the consequent deletion of the putative CO_2 gradient, on fluid transport. Benzolamide, a slowly permeant CA inhibitor, and a dextran-bound acetazolamide (mol wt 7,000) inhibit fluid transport by 28.8% and 22.8%, respectively (Fig. 5). Benzolamide has been reported to equilibrate slowly in human red blood cells at a rate of ~7%/h (39) and thus might also act on intracellular CA. We therefore ran a series of experiments in which we initiated the inhibition of fluid transport and stromal swelling with benzolamide and then followed with a solution containing CA. This should lead to an immediate reduction of benzolamide to nanomolar levels and thus should return fluid transport to control levels. The swelling ceased immediately (Fig. 5), indicating that the action of benzolamide was extracellular, although corneal thickness did not return completely to control levels. Consistently, the effect of inhibition of CA IV on fluid transport shown here (~20–30%) is significantly less than the known effect of inhibiting both CA IV and CA II, which was ~40–60% (12). In summary, slowly permeant or impermeant inhibitors of CA indeed reduce transendothelial fluid transport, but the inhibition is <30% of control (Fig. 5). In addition, as mentioned above, inhibition of Cl^- channels resulted in at most a 16% decrease of fluid transport (Fig. 4). It is interesting that the effects of impermeant and permeant CA inhibitors are additive. This is consistent with separate effects on an intracellular CA II and an extracellular CA IV, as discussed below.

In conclusion from the two segments above, from our evidence, inhibition of the two apical pathways previously proposed for anion efflux by Bonanno and colleagues, Cl^- channels (36, 43) and CO_2 flux (6, 8), even if combined together, cannot account for more than 40–45% of the baseline rate of transendothelial fluid transport. In the CO_2 gradient hypothesis above (6, 8), the intracellular CA II would mediate HCO_3^- dehydration and the extracellular CA IV HCO_3^- hydration. However, the function of luminal and interstitial CA IV described for kidney proximal tubule (40) and for gastric parietal cells (39) is dehydration of HCO_3^-, whereas the function of intracellular anhydrase is postulated to be hydration. In the scheme we propose below for the tandem of CAs in corneal endothelium, the enzymes function as proposed for the kidney and stomach.

Localization of NBC. We have demonstrated with confocal microscopy that in both cultured corneal endothelial cells and endothelial cells of freshly dissected cornea NBC proteins are located at the basolateral membrane and the apical membrane. As shown in Fig. 8, the density of staining at the apical membrane is significantly less than that at the basolateral membrane. This difference in the density of transport proteins is consistent with the HCO_3^- permeability of the apical membrane, which reportedly is four to three times lower than that of the basolateral membrane (8). If, in addition, the apical NBC transporter moves three molecules of HCO_3^- per turnover compared with two molecules per turnover of the basolateral NBC, then an apical protein density of 17–22% of that in the basolateral membrane may be expected.

The distribution of NBC isoform(s) to both the basolateral and apical cell membranes reported here poses the question of how the cell can be polarized so as to generate vectorial HCO_3^- flux under such conditions. In this connection, NBC is distributed throughout the basolateral and apical membrane domains in cultured bovine endothelial cells and freshly dissected rabbit corneal preparations. Such distribution has also been observed recently in the ducts of the submandibular glands of the rat (32). However, in these duct cells there appears to be a gradient of distribution that changes from a purely basolateral localization in the proximal sections of the submandibular ducts to localization in both basolateral and apical membrane domains and then to apical localization only in the distal parts of the duct. In the corneal endothelium and in cultured bovine endothelial cells simultaneous basolateral and apical fluorescence is seen consistently in all cells, as shown in Figs. 6–8. Our finding is in contrast prima facie to the observation by Sun et al. (37) and Bok (5), who report that indirect fluorescence, due to antibody binding, is confined to the basolateral membrane. However, the analysis of the data was somewhat different. We used three-dimensional reconstruction of the confocal images to show the antibody distribution in cross sections of the cultured bovine endothelial cells, whereas Sun et al. (37) examined optical slices in the *x-y* plane only. In addition, we obtained cryosections of the freshly dissected corneal endothelium, again to visualize the antibody distribution in cell cross sections. Finally, there is a large difference in protein density between the apical and basolateral membrane domains, which might have led other investigators to consider the apical staining insignificant. For this and other reasons, it will be relevant to attempt to explore the putative function of the newly described apical NBC.

Thermodynamics of net transcellular HCO_3^- flux. From the preceding arguments, our results suggest that NBCs are expressed in both apical and basolateral membrane domains. Under these conditions, vectorial HCO_3^- transport across the endothelium via NBCs can occur either if different NBC isoforms are located on the apical and basolateral membranes or if the same isoform exists but functions differently. One of these isoforms would require a stoichiometry of 2 HCO_3^-:1 Na^+ or less for HCO_3^- influx across the basolateral membrane, whereas the other would require a stoichiometry of 3 HCO_3^-:1 Na^+ or greater for HCO_3^- efflux across the apical membrane. There is a conceivable alternative in which the NBC would function with the same 2:1 stoichiometry on both cell sides. In that case, HCO_3^- would be transported into the cell from both sides and high cell HCO_3^- could drive the reaction $HCO_3^- + H^+ > CO_2 + H_2O$, with CO_2 rapidly diffusing across the apical membrane. However, as mentioned above, for such vectorial diffusion of CO_2 (Bonanno's hypothesis), there would have to be an apical extracellular CA IV reducing the extracellular CO_2 by hydration; only thus could there be a basolateral-to-apical CO_2 gradient and a net flow of CO_2. Our results this far do not support that view; inhibition of an apical extracellular CA IV (Fig. 5) with the consequent removal of the hypothetical CO_2 gradient reduces fluid transport by at most 29%. From the 16% inhibition of fluid transport (Fig. 4) seen in blocking apical anion channels, the expected inhibition of fluid transport, if due to CO_2 flow, would be some 84% instead.

Figure 9 describes the thermodynamic limits of the operating range for a system consisting of NBCs with 2:1 and 3:1

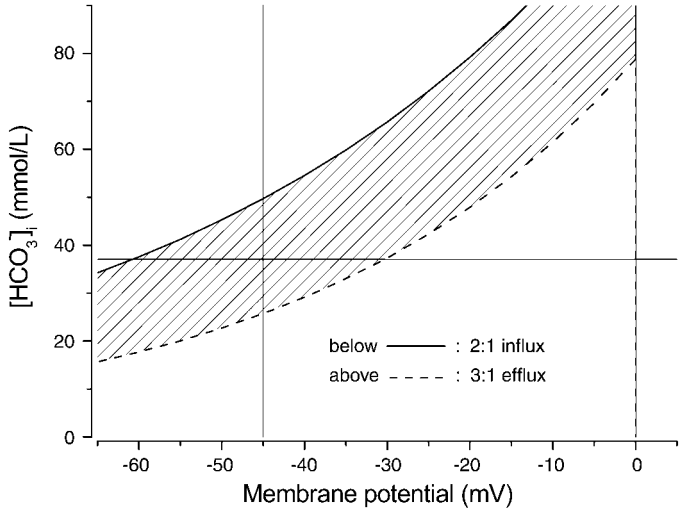

Fig. 9. Thermodynamics for flows across NBC. The curves represent limiting intracellular HCO_3^- ($[HCO_3^-]_i$; B_i) values obtained solving the equation $RT \ln (N_i/N_o) + z_N F(V_i - V_o) + n[RT \ln (B_i/B_o) + z_B F(V_i - V_o)] = 0$, where N_i is intracellular $[Na^+]$ (set at 15 mM), N_o is extracellular $[Na^+]$ (set at 145 mM), V_i is intracellular potential (independent variable), V_o is extracellular potential (set at 0), B_o is extracellular $[HCO_3^-]$ (set at 37 mM), B_i is $[HCO_3^-]_i$ (dependent variable), z is equivalents per mole, and the subscripts N and B refer to sodium and bicarbonate ions, respectively, and R, T, and F have their usual meanings. We solved for $B_i = f(V_i)$ at the 2 stoichiometries considered, $n = 2$ (*top curve*) and $n = 3$ (*bottom curve*). The vertical line corresponds to an intracellular potential of −45 mV (24). The horizontal line corresponds to a hypothetical $[HCO_3^-]_i$ of 37 mM. The curves mark limiting values for $[HCO_3^-]_i$. Above the *top curve*, there will be no net basolateral influx via a NBC at 2:1. Similarly, below the *bottom curve*, there will be no net apical efflux via a NBC at 3:1.

stoichiometries. According to this figure, net HCO_3^- flux could take place over a relatively wide range of membrane potential and intracellular $[HCO_3^-]$ ($[HCO_3^-]_i$) values, namely −30 to −61 mV at 37 mM $[HCO_3^-]_i$ and 26–50 mM $[HCO_3^-]_i$ at −45 mV membrane potential. These values fall within the physiologically expected range for an endothelial layer.

Identity of NBC isoforms. The expression of two different isoforms, a pancreatic (pNBC-1) and a kidney (kNBC-1) isoform, in corneal endothelium has been described by one group of investigators (41). However, Sun et al. (37) were able to identify only the presence of pNBC in cultured endothelial cells and freshly dissected corneal endothelia. Curiously, Lane et al. (23) were unable to identify either isoform in cultured endothelial cells. The antibody used in our studies does not distinguish between the pancreatic and kidney isoforms and therefore does not provide any information about the specific isoform(s) in our preparation. Still, there is another possibility. Recently it was reported that the kNBC-1 isoform, which extrudes HCO_3^- from proximal tubule cells at a 3:1 stoichiometry, exhibits 2:1 stoichiometry when expressed in *Xenopus* oocytes (16, 34). It has been suggested as a possible explanation for these observations that the stoichiometry of rat kNBC is determined by the absence or presence of an accessory protein (34). Another report (14) demonstrated that phosphorylation of a specific serine residue of the kNBC of murine tubule cells can shift its stoichiometry from 2:1 to 3:1. Therefore, it seems conceivable that tissue-dependent expression and translocation to specific membrane domains might thus allow the same NBC isoform to be used for HCO_3^- influx across the basolateral membrane and efflux across the apical membrane of the same cell.

An alternate transcellular anion transport model for corneal endothelial cells. On the basis of the data presented here, we propose a new model of transcellular anion transport across corneal endothelial cells (Fig. 10). In this model HCO_3^- enters the cell across the basolateral membrane via a NBC with a stoichiometry of 2 HCO_3^-:1 Na^+ (7). In parallel to this influx is a significantly smaller entry of Cl^- ions via the NKCC (9) and the anion exchanger. We propose that the anion efflux through the apical membrane is predominantly due to a NBC with a ratio of 1 Na^+:3 HCO_3^- and a smaller Cl^- efflux through Cl^- channels. An apical NBC mediating HCO_3^- efflux is in line with evidence for Na^+-HCO_3^- coupled exit cited above for cultured corneal endothelial cells (20). As Fig. 9 shows, a 3:1 NBC would operate relatively close to the thermodynamic limit. However, as hypothesized in Fig. 10, the combined action of the intracellular CA II and extracellular CA IV working in tandem would create/enhance a local $[HCO_3^-]$ gradient across the apical membrane to facilitate efflux across the NBC. The intracellular CA II would catalyze the conversion of CO_2 to HCO_3^-, whereas the membrane-bound extracellular CA IV would catalyze the reverse reaction. This is consistent with recent proposals that CA II is bound to the COOH terminal of NBC-1 in kidney proximal tubule (35); such binding apparently takes place only when the NBC is dephosphorylated and hence working in the 3:1 mode (15). There is also evidence that CA II and CA IV are tethered in

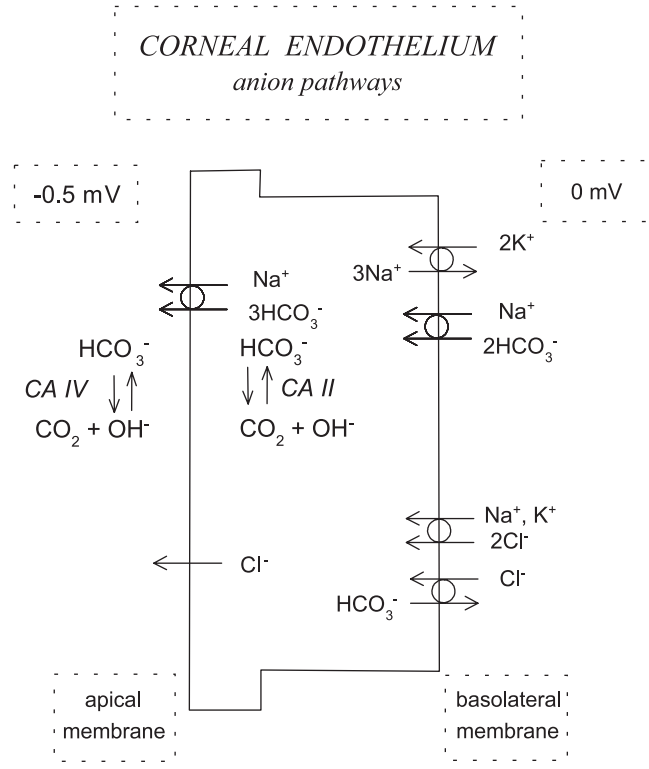

Fig. 10. Scheme of the pathways proposed for anion passage across corneal endothelium. All membrane proteins involved are cotransporters/exchangers except for the Cl^- channel. The CAs may be tethered to and operating in tandem with the apical NBC. Although not a direct part of the anion routes, the Na^+ pump creates the necessary gradients; it is shown for reference.

close proximity to NBC extracellular and intracellular sites, respectively, in NBC-1-transfected HEK293 cells (3).

GRANTS

This work was supported by National Eye Institute Grant EY-06178 (J. Fischbarg) and by Research to Prevent Blindness, Inc.

REFERENCES

1. **Aboalchamat B, Engelmann K, Bohnke M, Eggli P, and Bednarz J.** Morphological and functional analysis of immortalized human corneal endothelial cells after transplantation. *Exp Eye Res* 69: 547–553, 1999.
2. **Akiyama R, Kuang K, Chiaradia P, Roberts CW, and Fischbarg J.** Effects of acetylcholine, carbachol and mannitol on rabbit corneal endothelial function as assessed by corneal deturgescence. *Graefes Arch Clin Exp Ophthalmol* 235: 384–387, 1997.
3. **Alvarez BV, Loiselle FB, Supuran CT, Schwartz GJ, and Casey JR.** Direct extracellular interaction between carbonic anhydrase IV and the human NBC1 sodium/bicarbonate co-transporter. *Biochemistry* 42: 12321–12329, 2003.
4. **Barfort P and Maurice DM.** Electrical potential and fluid transport across the corneal endothelium. *Exp Eye Res* 19: 11–19, 1974.
5. **Bok D, Schibler MJ, Pushkin A, Sassani P, Abuladze N, Naser Z, and Kurtz I.** Immunolocalization of electrogenic sodium-bicarbonate cotransporters pNBC1 and kNBC1 in the rat eye. *Am J Physiol Renal Physiol* 281: F920–F935, 2001.
6. **Bonanno JA.** Identity and regulation of ion transport mechanisms in the corneal endothelium. *Prog Retin Eye Res* 22: 69–94, 2003.
7. **Bonanno JA and Giasson C.** Intracellular pH regulation in fresh and cultured bovine corneal endothelium. II. Na^+:HCO_3^- cotransport and Cl^-/HCO_3^- exchange. *Invest Ophthalmol Vis Sci* 33: 3068–3079, 1992.
8. **Bonanno JA, Guan Y, Jelamskii S, and Kang XJ.** Apical and basolateral CO_2-HCO_3^- permeability in cultured bovine corneal endothelial cells. *Am J Physiol Cell Physiol* 277: C545–C553, 1999.
9. **Diecke FPJ, Zhu Z, Kang F, Kuang K, and Fischbarg J.** Sodium, potassium, two chloride cotransport in corneal endothelium: characterization and possible role in volume regulation and fluid transport. *Invest Ophthalmol Vis Sci* 39: 104–110, 1998.
10. **Dikstein S and Maurice DM.** The metabolic basis of the fluid pump in the cornea. *J Physiol* 221: 29–41, 1972.
11. **Fischbarg J.** Potential difference and fluid transport across rabbit corneal endothelium. *Biochim Biophys Acta* 228: 362–366, 1972.
12. **Fischbarg J and Lim JJ.** Role of cations, anions and carbonic anhydrase in fluid transport across rabbit corneal endothelium. *J Physiol* 241: 647–675, 1974.
13. **Fischbarg J, Lim JJ, and Bourguet J.** Adenosine stimulation of fluid transport across rabbit corneal endothelium. *J Membr Biol* 35: 95–112, 1977.
14. **Gross E, Hawkins K, Pushkin A, Sassani P, Dukkipati R, Abuladze N, Hopfer U, and Kurtz I.** Phosphorylation of Ser^{982} in the sodium bicarbonate cotransporter kNBC1 shifts the HCO_3^-: Na^+ stoichiometry from 3:1 to 2:1 in murine proximal tubule cells. *J Physiol* 537: 659–665, 2001.
15. **Gross E, Pushkin A, Abuladze N, Fedotoff O, and Kurtz I.** Regulation of the sodium bicarbonate cotransporter kNBC1 function: role of Asp^{986}, Asp^{988} and kNBC1-carbonic anhydrase II binding. *J Physiol* 544: 679–685, 2002.
16. **Heyer M, Muller-Berger S, Romero MF, Boron WF, and Fromter E.** Stoichiometry of the rat kidney Na^+-HCO_3^- cotransporter expressed in *Xenopus laevis* oocytes. *Pflügers Arch* 438: 322–329, 1999.
17. **Hodson S.** The regulation of corneal hydration by a salt pump requiring the presence of sodium and bicarbonate ions. *J Physiol* 236: 271–302, 1974.
18. **Hodson S and Miller F.** The bicarbonate ion pump in the endothelium which regulates the hydration of the rabbit cornea. *J Physiol* 263: 563–577, 1976.
19. **Hull DS, Green K, Boyd M, and Wynn HR.** Corneal endothelial bicarbonate transport and the effect of carbonic anhydrase inhibitors on endothelial permeability, fluxes and thickness. *Invest Ophthalmol Vis Sci* 16: 883–892, 1977.
20. **Jentsch TJ, Keller SK, Koch M, and Wiederholt M.** Evidence for coupled transport of bicarbonate and sodium in cultured bovine corneal endothelial cells. *J Membr Biol* 81: 189–204, 1984.
21. **Kuang K, Li Y, Wen Q, Wang Z, Li J, Yang Y, Iserovich P, Reinach PS, Sparrow J, Diecke FPJ, and Fischbarg J.** Corneal endothelial Na^+-K^+-$2Cl^-$ cotransporter: molecular identification, location, and contribution to fluid transport. *Am J Physiol Cell Physiol* 280: C491–C499, 2001.
22. **Kuang K, Xu M, Koniarek JP, and Fischbarg J.** Effects of ambient bicarbonate, phosphate and carbonic anhydrase inhibitors on fluid transport across rabbit corneal endothelium. *Exp Eye Res* 50: 487–493, 1990.
23. **Lane J, Wigham CG, and Hodson SA.** A chloride-activated Na^+/HCO_3^--coupled transport activity in corneal endothelial membranes. *Biophys J* 78: 2493–2498, 2000.
24. **Lim JJ and Fischbarg J.** Intra-cellular potential of rabbit corneal endothelial cells. *Exp Eye Res* 28: 619–626, 1979.
25. **Lytle C, Xu JC, Biemesderfer D, and Forbush B 3rd.** Distribution and diversity of Na-K-Cl cotransport proteins: a study with monoclonal antibodies. *Am J Physiol Cell Physiol* 269: C1496–C1505, 1995.
26. **Ma T, Thiagarajah JR, Yang H, Sonawane ND, Folli C, Galietta LJ, and Verkman AS.** Thiazolidinone CFTR inhibitor identified by high-throughput screening blocks cholera toxin-induced intestinal fluid secretion. *J Clin Invest* 110: 1651–1658, 2002.
27. **Maurice DM.** The location of the fluid pump in the cornea. *J Physiol* 221: 43–54, 1972.
28. **McLean IW and Nakane PK.** Periodate-lysine-paraformaldehyde fixative. A new fixation for immunoelectron microscopy. *J Histochem Cytochem* 22: 1077–1083, 1974.
29. **Narula PM, Xu M, Kuang K, Akiyama R, and Fischbarg J.** Fluid transport across cultured bovine corneal endothelial cell monolayers. *Am J Physiol Cell Physiol* 262: C98–C103, 1992.
30. **Rae JL and Watsky MA.** Ionic channels in corneal endothelium. *Am J Physiol Cell Physiol* 270: C975–C989, 1996.
31. **Ridderstrale Y, Wistrand PJ, and Brechue WF.** Membrane-associated CA activity in the eye of the CA II-deficient mouse. *Invest Ophthalmol Vis Sci* 35: 2577–2584, 1994.
32. **Roussa E, Romero MF, Schmitt BM, Boron WF, Alper SL, and Thevenod F.** Immunolocalization of anion exchanger AE2 and Na^+-HCO_3^- cotransporter in rat parotid and submandibular glands. *Am J Physiol Gastrointest Liver Physiol* 277: G1288–G1296, 1999.
33. **Sanchez JM, Li Y, Rubashkin A, Iserovich P, Wen Q, Ruberti JW, Smith RW, Rittenband D, Kuang K, Diecke FPJ, and Fischbarg J.** Evidence for a central role for electro-osmosis in fluid transport by corneal endothelium. *J Membr Biol* 187: 37–50, 2002.
34. **Sciortino CM and Romero MF.** Cation and voltage dependence of rat kidney electrogenic Na^+-HCO_3^- cotransporter, rkNBC, expressed in oocytes. *Am J Physiol Renal Physiol* 277: F611–F623, 1999.
35. **Soleimani M.** Na^+:HCO_3^- cotransporters (NBC): expression and regulation in the kidney. *J Nephrol* 15, *Suppl* 5: S32–S40, 2002.
36. **Sun XC and Bonanno JA.** Expression, localization, and functional evaluation of CFTR in bovine corneal endothelial cells. *Am J Physiol Cell Physiol* 282: C673–C683, 2002.
37. **Sun XC, Bonanno JA, Jelamskii S, and Xie Q.** Expression and localization of Na^+-HCO_3 cotransporter in bovine corneal endothelium. *Am J Physiol Cell Physiol* 279: C1648–C1655, 2000.
38. **Sun XC, McCutheon C, Bertram P, Xie Q, and Bonanno JA.** Studies on the expression of mRNA for anion transport related proteins in corneal endothelial cells. *Curr Eye Res* 22: 1–7, 2001.
39. **Swenson ER, Tewson TW, Wistrand PJ, Ridderstrale Y, and Tu C.** Biochemical, histological, and inhibitor studies of membrane carbonic anhydrase in frog gastric acid secretion. *Am J Physiol Gastrointest Liver Physiol* 281: G61–G68, 2001.
40. **Tsuruoka S, Swenson ER, Petrovic S, Fujimura A, and Schwartz GJ.** Role of basolateral carbonic anhydrase in proximal tubular fluid and bicarbonate absorption. *Am J Physiol Renal Physiol* 280: F146–F154, 2001.
41. **Usui T, Seki G, Amano S, Oshika T, Miyata K, Kunimi M, Taniguchi S, Uwatoko S, Fujita T, and Araie M.** Functional and molecular evidence for Na^+-HCO_3^- cotransporter in human corneal endothelial cells. *Pflügers Arch* 438: 458–462, 1999.
42. **Van Adelsberg J, Edwards JC, Herzlinger D, Cannon C, Rater M, and Al-Awqati Q.** Isolation and culture of HCO_3^--secreting intercalated cells. *Am J Physiol Cell Physiol* 256: C1004–C1011, 1989.
43. **Zhang Y, Xie Q, Sun XC, and Bonanno JA.** Enhancement of HCO_3^- permeability across the apical membrane of bovine corneal endothelium by multiple signaling pathways. *Invest Ophthalmol Vis Sci* 43: 1146–1153, 2002.